Quantitative three-dimensional imaging of chemical short-range order via machine learning enhanced atom probe tomography *Supplementary*: Atomistic simulations

L. Huber[1] R. Dsouza[1] J. Neugebauer[1]

[1]Max-Planck-Institut für Eisenforschung GmbH, D-40237 Düsseldorf, Germany

November 4, 2021

1 Introduction

In the main manuscript, we demonstrate that the machine learning (ML) approach can successfully identify short-range-ordering (SRO) in an Fe-Al alloy with nominal Al concentration around 18%at. Applying this methodology to APT tips annealed at 873 K and 523 K, we have searched for both $D0_3$ and B2 SRO clusters. Experimentally, there we find no evidence for $D0_3$ clustering beyond that expected to happen by random chance (i.e. "statistical clustering") at either temperature. For B2 , although the absolute number of clusters is small, we do see experimental evidence for such SRO at the lower annealing temperature of 523 K. Can these observations be replicated using atomistic simulations? Since such simulations are much less expensive than physical experiments, if simulations are found to agree with experiment at the two available temperatures, this would give us confidence to scan the entire interpolating temperature regime much more densely to look for trends and regions of transition. In the event that simulations do not match experiment, are there still lessons to be learned about the underlying mechanisms that drive SRO in this system?

This problem can be attacked directly using coupled Monte Carlo / Molecular Dynamics (MCMD) calculations which allow a system of comparable size to the experimental domain to equilibrate chemically. Such calculations allow all factors contributing to the classical free energy – potential energy, vibrational entropy, and configurational entropy – to be directly

present in the simulation and competing, and if the total free energy favours SRO this will appear naturally. However, the downside of such powerful simulations is that they are too expensive to perform using first principles calculations with any respectable simulation domain, so we need to restrict ourselves to classical empirical potentials. To this end, we survey all four available embedded atom method (EAM) and modified EAM (MEAM) potentials publicly available on the NIST potential repository [1]. Using each potential to build a simple approximation of free energies for the relevant Fe-Al phases allows us to immediately rule out two potentials. For the remaining two we run MCMD calculation and apply a clustering algorithm to look for the presence and distribution of $D0_3$ and B2 SRO/precipitation. None of our potentials are able to reproduce the experimental results, but for one we are able to see $D0_3$ SRO beyond what is expected statistically. This clustering behaviour is enhanced at the higher annealing temperature, and the full atomic-scale resolution of the simulations allow us to suggest a mechanism for this behaviour and a path to driving such SRO in practice.

2 Computational details

All calculations were performed within the `pyiron` [2, 3] framework driving `LAMMPS` [4, 5] to evaluate forces and energies and run the molecular dynamics calculations. The coupled Monte Carlo/MD calculations were performed using the Variance-Constrained Semi-Grand-Canonical (VCSGC) framework provided as a `fix` in `LAMMPS` by Sadigh *et al.* [6, 7]. The atomic interactions are described by the embedded atom method (EAM) potentials of Mendelev *et al.* [8] and Farkas and Caro [9], and the modified EAM (MEAM) potentials of Lee and Lee [10] and Jelenik *et al.* [11]. The full code for reproducing these results (at least stochastically) can be found on `github` [12].

3 Results

We begin by performing a very simple screening of the available potentials using 0 K potential energy calculations. The energy for the relevant ideal Fe-Al phases is shown in Fig. 1. Here we can already see that the potentials of Farkas *et al.* [9] and Jelinek *et al.* [11] both fail to provide clear BCC stability. This is not shocking as these were both designed for high-entropy alloys, and the former is explicitly targeted towards the FCC phase. Nonetheless, for the rest of our investigation we can safely focus on the EAM potential of Mendelev *et al.* [8] and the more recent MEAM potential of Lee and Lee *et*

al. [10].

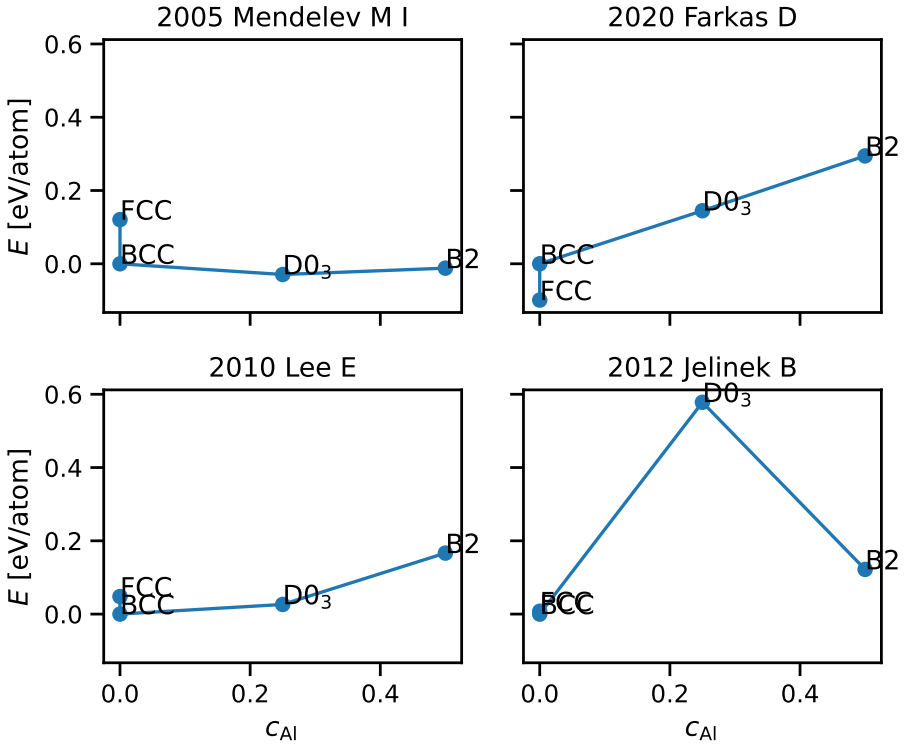

Figure 1: 0K potential energy/atom for each of the relevant Fe-Al phases up to 50% Al for several empirical potentials [8, 10, 11, 9].

In addition to being BCC stable, we know that the potentials should be dominated by a solid solution at 18% Al, and that at higher concentrations the $D0_3$ phase should also be energetically competitive. To this end, the expanded diagram in Fig. 2 to include the random solid solution energy at Al concentrations up to the nominal $D0_3$ concentration. At each concentration ten different random configurations of 432 atoms ($6 \times 6 \times 6$ BCC units) we relaxed at zero pressure, and the final energy averaged over. The error bars for the solid solution shows the 95% confidence interval from the sampling (i.e. roughly double the standard deviation). During our exploration we discovered that the Mendelev potential actually shows a strong preference for alternative ordered structures with columnar and planar Al. We included these configurations at different Al concentration by varying

their inter-columnar or inter-planar spacing. Representatives of all of these are visualized in Fig. 3.

In addition to the 0 K potential energy, for the BCC solid solution, the ideal entropy of mixing was included at both the experimental annealing temperatures. This demonstrates the increasing benefit to the *free* energy for the system to occupy a disordered state. In principle the entropy of mixing is also relevant for the other phases – even our SRO clusters may contain chemical antisites and do not need to *perfectly* conform to the reference ordering – but at this stage they are omitted, as is vibrational entropy for all phases. Even with these simplifications, we can already draw important conclusions: first, the Mendelev potential will never display $D0_3$ SRO at 18% Al, and indeed even at the nominal $D0_3$ concentration of 25% Al it is *still* not the preferable state for this potential – by constructing a parallel tangent line between the minima of the phases, we can expect the system is likely to form either a composition of solid solution and the layered structure, or simply form into ordered layers. The potential energy of this layered structure sits so far below the $D0_3$ phase that we should never expect to see $D0_3$ form in any significant fraction. Second, B2 formation is similarly unlikely at the nominal alloy composition, although the preference for planar and columnar Al configurations can be interpreted as colmnar or planar B2 (which is not what was found experimentally, where B2 SRO clusters are generally spherical). The third key observation is that for the Lee potential a similar Gibbs-tie-line analysis shows that decomposition into solid solution and $D0_3$ *is* possible, but may only occur at higher temperatures than we expect from experiment – at the lower temperature of 523 K we can also expect a decomposition into BCC and $D0_3$, but with almost no Al in the BCC solution. I.e. this potential seems to have an unphysically low solubility of Al in bulk BCC Fe. Finally, for the Lee potential we also do not expect any B2 SRO.

Next, to allow the full interplay and competition of all factors including vibrational entropy, we perform full MCMD calculations using the variance constrained approach [6, 7] (with a relatively strict constraint $\kappa = 1e4$) to maintain the Al concentration very close to the nominal experimental value of 18%. Estimating the chemical potential, $\Delta\mu$ from the change in 0 K potential energies of the most favourable phases – BCC and $D0_3$ (layered Al) for the Lee (Mendelev) potential – gives $|\Delta\mu| < 0.1$ eV (< 0.3 eV) for the Lee (Mendelev) potential. As seen by the inclusion of just configurational entropy to the solid solution phase, this is very likely to be an upper bound to the true chemical potential, as point defects in the secondary phase would lower its free energy and further reduce the slope of any Gibbs tie line.

Since the application of the variance constraint means that the chemical potential does not ultimately influence the nature of the results obtained but only the computational efficiency (i.e. number of MC steps required) we safely approximate $\Delta\mu = 0$ for both potentials. With a 1 fs timestep for integration, these simulations ran for 100 ps each, with MC trial swaps for 10% of the atoms every 0.1 ps. Although smaller than the experimental dimensions, the simulation cells were of the same order of magnitude: $4 \times 4 \times 4$ nanometer periodic cubes (5488 atoms) in a periodic domain. We can get a quick sense of whether the system has converged to the desired chemical ordering by examining the equilibration of the potential energy as a function of time/MC steps. This is shown in Fig. 4 where we see that all systems except for the Lee potential at 523 K have converged to fluctuate around the average energy of the back half of the simulation. In contrast, the Lee potential at 523 K still shows a clear trend of decreasing energy, indicating that it has not reached its equilibrium configuration at all. This slow convergence can be understood in light of Fig. 2, since at this temperature we are most likely in a miscibility gap between very low concentration solid solution and $D0_3$; starting from an initial configuration of random solid solution with 18% Al, the system is trying to decompose into pure $D0_3$ and BCC with almost no Al, a process which requires many, many MC swaps.

Unlike the experimental APT data, we have full access to the species and position of each atom in our computational sample. Thus, to analyze SRO into the specific $D0_3$ and B2 configurations observed in experiment, we can directly check whether each atom has a local environment that matches the target phase. We do this by constructing the topology of our system considering all 14 first- and second-nearest neighbours (NN) to be "connected", and comparing the species of the atom under question as well as all of its neighbours to one of six references: two from the B2 pattern with Al occupying either simple-cubic sublattice, and four symmetry-equivalent organizations of $D0_3$. Using a breadth-first-search, for each of the six reference patterns we construct all matching clusters.

The size and number of clusters found is then dependent on how strictly we demand that the test environment match the reference environment; if we very strictly insist that each atom in a cluster be surrounded by *exactly* the reference cluster, it is more difficult to find clusters beyond a few atoms in size given the entropic favourability of point defects in the secondary phase; however, at the opposite extreme, if we are too relaxed in our condition and allow atoms with only a few neighbours matching the reference to count towards a cluster, then the entire system is consumed with one erroneous

"cluster". To overcome this we must make reference to the same clustering algorithm applied to the truly random solid solution used as input to the MCMD simulations, and consider the *changes* in the cluster distribution after the sample has been allowed to equilibrate its chemical ordering. We found that a threshold value of 13 of the 14 NN gives us gives good resolution for contrasting the random sample – where clusters may occur by pure chance – and the MCMD annealed samples – where clusters may still occur by pure chance, but also may form due to a driving force for SRO. The interested reader can examine the `github` repository [12] for more detail.

The resulting histograms for identified clusters – ignoring *single atom* "clusters" and binning by ten atoms at a time – can be seen in Figs. 5 and 6 for the Mendelev and Lee potentials, respectively. The Mendelev potential shows a very mild decrease in $D0_3$ clusters, suggesting that the small random clusters may have some small driving force to group together into fewer, very slightly larger clusters. For B2 the opposite effect is seen, but it is clear from examining the total number of clusters that this is trivial. At neither temperature and for neither reference phase does the Mendelev potential exhibit SRO to either of the relevant phases.

Meanwhile, the Lee potential shows a similar non-result for B2 ordering, but we observe a distinct trend for SRO of $D0_3$ clusters, especially at the higher temperature. At 523 K we see one medium sized cluster (about 50 atoms) and ten small clusters in the 10-20 atom range, but this calculation was poorly converged. At 873 K the calculation was well converged and here we see four large clusters (¿100 atoms, where the binning is truncated), as well as a collection of medium sized clusters, and some small clusters. Note that this histogram is truncated at a size of 100, so the four counts at the largest size are actually all different sizes, each some hundreds of atoms.

By referring back to Fig. 2, we can see that we expect to be in the miscibility gap between the solid solution and $D0_3$ phases. So, at 873 K where we see the formation of a whole distribution of clusters, are we really at a thermodynamic equilibrium or is this merely a transient state on the path to perfect phase separation? Even though we are inside a miscibility gap, and ignoring unlikely scenarios like a negative solid solution/$D0_3$ interface energy, there is still a clear explanation for why we may observe SRO instead of *only* decomposition: while the system still wants to form $D0_3$, there at higher temperatures there is an increased entropic benefit to allowing this $D0_3$ to occur in many small clusters spread throughout the system instead of by full phase separation. In the classic image of a TTT diagram, we may be up above the nose, where the formation of a precipitate above the critical size for Ostwald ripening (i.e. completely stable against decomposition)

becomes exceedingly unlikely – or at least takes a very long time. Since the MCMD infrastructure is not well-optimized for MEAM potentials like the Lee potential, simply running much longer is not a desirable solution.

One alternative approach is to change our MCMD initial conditions by *starting* from perfect phase separation instead of starting from random solution. In this case, at high temperature we expect this perfect $D0_3$ precipitate to decompose to bring the solid solution equilibrium value and then to still see the formation of new $D0_3$ SRO clusters forming in the BCC domain. At the lower temperature, in contrast, our earlier calculations with 0 K energy and configurational entropy indicate that the equilibrium concentration of Al in the BCC phase will be extremely low. Under these conditions it should be very difficult for enough Al to come together for short lived SRO clusters, and we expect little to no decomposition of the initial monolithic precipitate.

Here, we have used a (roughly) spherical $D0_3$ coherent precipitate in the pure-Fe BCC bulk, with the size of the precipitate tuned so that the Al concentration is still 18%. Results of the cluster analysis through time can be see in Fig. 7 at both temperatures – the single largest cluster of more than 4000 atoms is not shown. Indeed, at the lower temperature there is zero indication of any dissolution of the initial precipitate. Some of the intermediate steps show a change in cluster counts for the 2-10 atom range, which may occur as Al atoms swap into the BCC bulk for a transient existence as a point defect, but no other clusters form and survive and the final Al concentration in the BCC is still zero. The remaining small clusters occur because some Fe atoms are able to register as having a $D0_3$ -like environment while being perfectly surrounded by other Fe atoms. On the other hand, at 873 K, we see clear evidence that the precipitate is dissolving: there are dozens of small clusters (2-10 atoms) and one or two slightly larger clusters (20-30 atoms) throughout the simulation, and the final Al concentration in the BCC bulk is 4%. Just as the cold simulation starting from the random solution did not fully equilibrate, neither does the hot simulation starting from full phase decomposition, but the qualitative trend is completely consistent with our earlier observation of SRO in the high temperature-random start MCMD calculation.

If this entropically-driven perspective is correct, we should also see that the observed SRO clusters are not infinitely long lived, but eventually dissolve only to reform somewhere else. To study this, we can look at what fraction of sites identified as part of a $D0_3$ cluster are new, i.e. were not identified as $D0_3$ sites in the last snapshot of the system's evolution. This is shown in Fig. 8 at both low and high temperature for the Lee potential starting from random solid solution. Due to the large amount of MD time

(10 ps) and large number of trial MC swaps (10% of the system 100 times), we can expect the sequential snapshots to be quite well decorrelated.

By studying the system energy as a function of time back in Fig. 4 we know that the 523 K simulation is not well converged. With the additional data here we see that less than 20% of the $D0_3$ sites in each snapshot are new, and indeed this roughly corresponds to total number of additional sites as the system continues to phase decompose – i.e. at this low temperature we effectively have the formation and ripening of clusters. In contrast, although there is still some weak upwards trend in the total number of $D0_3$ sites, at 873 K we see that the phase transformation has more or less stabilized for the last five snapshots and the total sites identified as $D0_3$ is roughly constant. In this near-equilibrium regime, we see that fully *half* of the atoms participating in a $D0_3$ cluster are not preserved from snapshot to snapshot. This is completely consistent with our picture of the "rolling boil" of SRO precipitates forming, dissolving, and reforming at this high temperature.

As a bit of an aside, we can also test whether Fig. 2 makes accurate predictions for the Mendelev potential. Testing for columnar or planar precipitates is harder, because we do not have the same easy reference system to compare to. However, both these shapes can be thought of as a very particularly arranged B2 precipitate. By weakening our clustering criterion to 11 out of 14 NN and examining some of the larger B2 clusters identified, we can indeed locate the formation of small plate-like precipitates which support the planar phase, shown in Fig. 9(a) where one of the larger clusters is plotted for the equilibrated system at 523 K. Partial columns of Al are also clearly visible in the full structure, also shown in Fig. 9(b). As with the other structure plots, the atoms are always mapped back to their lattice positions, although their true atomic positions of the snapshot are disorderly as they are the output of an MD trajectory. Since the clusters identified by ML in the experimental samples appear to be roughly spherical, we believe this behaviour is just an artefact of the empirical potential and not an indication that it is more realistic than the Lee potential in this regime.

4 Conclusions

In an attempt to corroborate experimental evidence for SRO in Fe-Al, we have performed atomistic simulations using all four classical potentials publicly available on the NIST repository. By examining 0 K potential energies for various phases (including $T > 0$ K configurational entropy for the BCC

Fe-Al solid solution), we showed that two potentials could be ruled out immediately for not being BCC-stable [9, 11], one [8] showed an appropriate tendency towards solid solution but preferred planar- and columnar-Al organization over $D0_3$, and the last one [10] promisingly showed a small miscibility gap between moderately high Al-concentration solid solution and the expected abutting phase, $D0_3$ – at least at sufficiently high temperature.

By running full, coupled MCMD calculations to chemically equilibrate 64 nm^3 periodic cubes of Fe-18%at. Al, we found that the simplified 0 K energies (plus configurational entropy) provide a useful lens for interpreting observed clustering behaviour. Using an algorithm to identify contiguous domains matching reference $D0_3$ and B2 patterns reveals that the potential of Lee and Lee [10] does indeed show a strong tendency to form dozens of small cluster (¡20 atoms) as well as a handful of moderately sized clusters (40-270 atoms) at the higher temperature of 873 K. By using an alternative initial condition (perfect phase decomposition) and by studying the turnover of participation in $D0_3$ clusters, we showed that at the lower temperature of 523 K the system is driven towards perfect phase decomposition of $D0_3$ and almost pure-Fe BCC, with slow consistent growth of precipitates in the MCMD calculations. In contrast, the situation at 873 K can best be understood to lie above the nose of a TTT diagram; at this temperature the BCC solution retains a moderate amount of Al and clusters of various sizes readily form, dissolve, and reform later in a different location. Under no circumstances did our simulations give strong evidence of B2 SRO.

While we did not directly observe the formation of B2 SRO seen in experiment, these calculations do offer hints at the driving mechanisms for the experimentally observed behaviour. In our calculations, which are not constrained by diffusion kinetics, the lower annealing temperature has a tendency to allow Ostwald ripening of precipitates, while the higher temperature is entropically driven to maintain more and smaller clusters. These are equivalent to sitting inside and on top of the nose in a TTT diagram, respectively. In contrast, the experimental observation that SRO occurs at lower but not higher annealing temperatures suggests that perhaps the energetic driving force for forming these clusters is relatively small and easily overcome by the entropic benefit of disorder at the higher temperature, and that kinetic constraints may be preventing these fragile SRO clusters from ripening (i.e. we sit beneath the TTT nose). We do not have a conclusive explanation for why it is $D0_3$ ordering observed in our calculations while B2 ordering is observed experimentally, but it is always possible with empirical potentials that the simulations simply do not represent the interatomic interactions with sufficient fidelity. We can, however, suggest that $D0_3$ SRO

may be obtainable by increasing the nominal Al concentration (so there is more likely to be sufficient Al for local $D0_3$ regimes to form) and increasing the annealing temperature (to prevent such clusters from ripening).

Acknowledgements

Thanks to Tilmann Hickel for useful discussions.

References

[1] Nist. `https://www.ctcms.nist.gov/potentials/system/Fe/`, 2021.

[2] `pyiron`. `https://pyiron.org`, 2021.

[3] Jan Janssen, Sudarsan Surendralal, Yury Lysogorskiy, Mira Todorova, Tilmann Hickel, Ralf Drautz, and Jörg Neugebauer. pyiron: An integrated development environment for computational materials science. *Computational Materials Science*, 163:24 – 36, 2019.

[4] `LAMMPS`. `https://lammps.sandia.gov`, 2021.

[5] Steve Plimpton. Fast parallel algorithms for short-range molecular dynamics. *Journal of computational physics*, 117(1):1–19, 1995.

[6] Babak Sadigh and Paul Erhart. Calculation of excess free energies of precipitates via direct thermodynamic integration across phase boundaries. *Physical Review B*, 86(13):134204, 2012.

[7] Babak Sadigh, Paul Erhart, Alexander Stukowski, Alfredo Caro, Enrique Martinez, and Luis Zepeda-Ruiz. Scalable parallel monte carlo algorithm for atomistic simulations of precipitation in alloys. *Physical Review B*, 85(18):184203, 2012.

[8] MI Mendelev, David J Srolovitz, Graeme J Ackland, and Seungwu Han. Effect of fe segregation on the migration of a non-symmetric $\sigma 5$ tilt grain boundary in al. *Journal of materials research*, 20(1):208–218, 2005.

[9] Diana Farkas and Alfredo Caro. Model interatomic potentials for fe–ni–cr–co–al high-entropy alloys. *Journal of Materials Research*, 35(22):3031–3040, 2020.

[10] Eunkoo Lee and Byeong-Joo Lee. Modified embedded-atom method interatomic potential for the fe–al system. *Journal of Physics: Condensed Matter*, 22(17):175702, 2010.

[11] Bohumir Jelinek, Sebastien Groh, Mark F Horstemeyer, Jeffery Houze, Seong-Gon Kim, Gregory J Wagner, Amitava Moitra, and Michael I Baskes. Modified embedded atom method potential for al, si, mg, cu, and fe alloys. *Physical Review B*, 85(24):245102, 2012.

[12] Code repository. `https://github.com/liamhuber/FeAl_solution`, 2021.

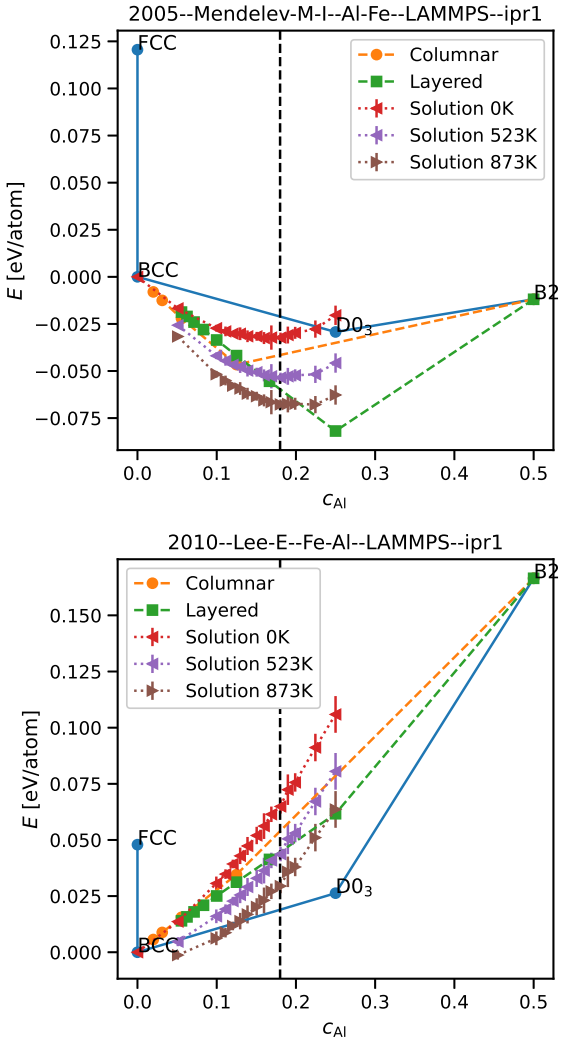

Figure 2: 0K potential energy/atom for the regular phases, but also columnar Al (orange circles), planar Al (green squares), and random solid solution including configurational entropy at three temperatures, 0 K, 523 K, and 873 K (triangles red, purple, and brown, respectively) with error bars showing a 95% confidence interval for the average solution energy.

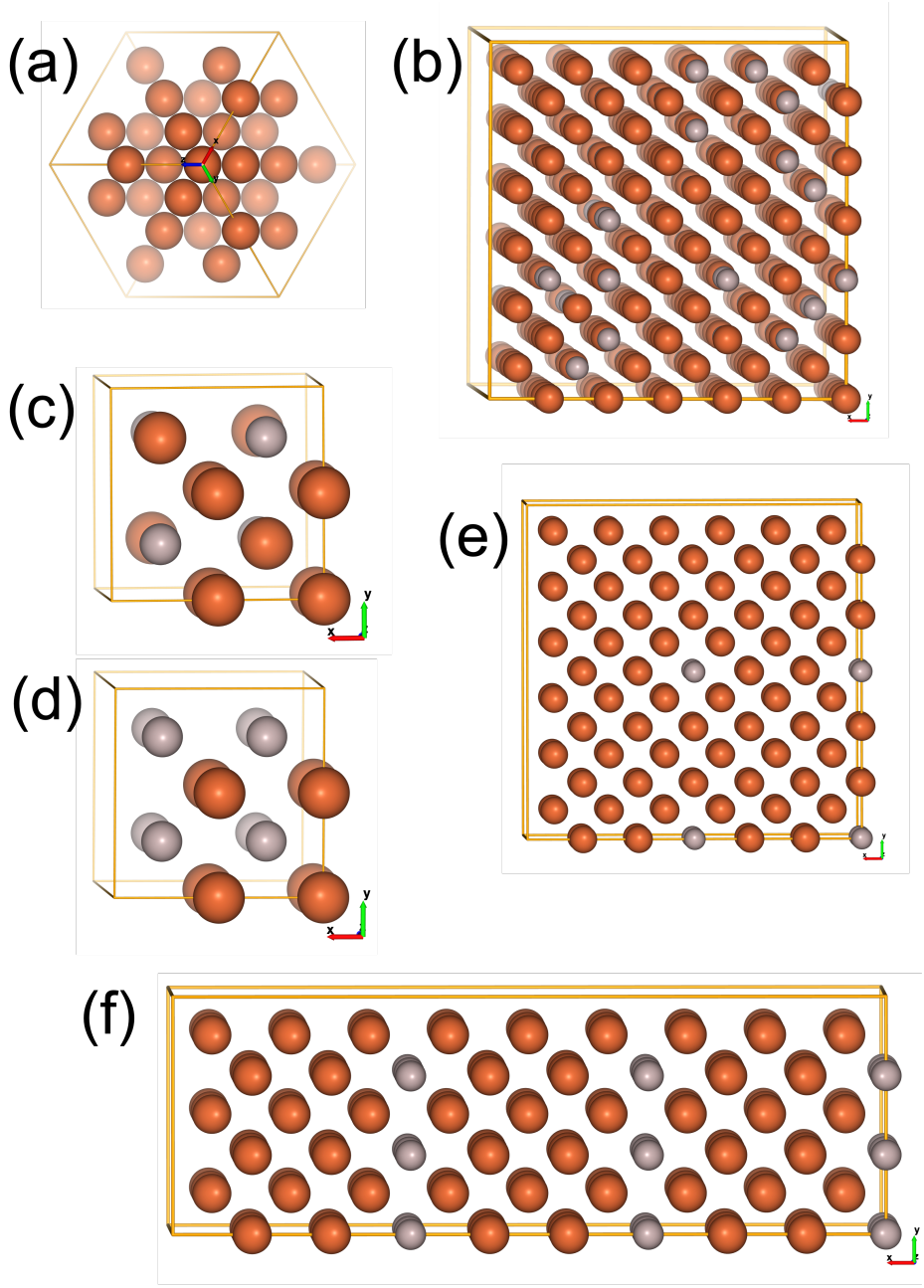

Figure 3: Representative visualizations of the structures for (a) FCC, (b) BCC (with 18% Al), (c) $D0_3$, (d) B2 , (e) the columnar structure, and (f) the planar structure. Al is shown small and grey while Fe is larger and red.

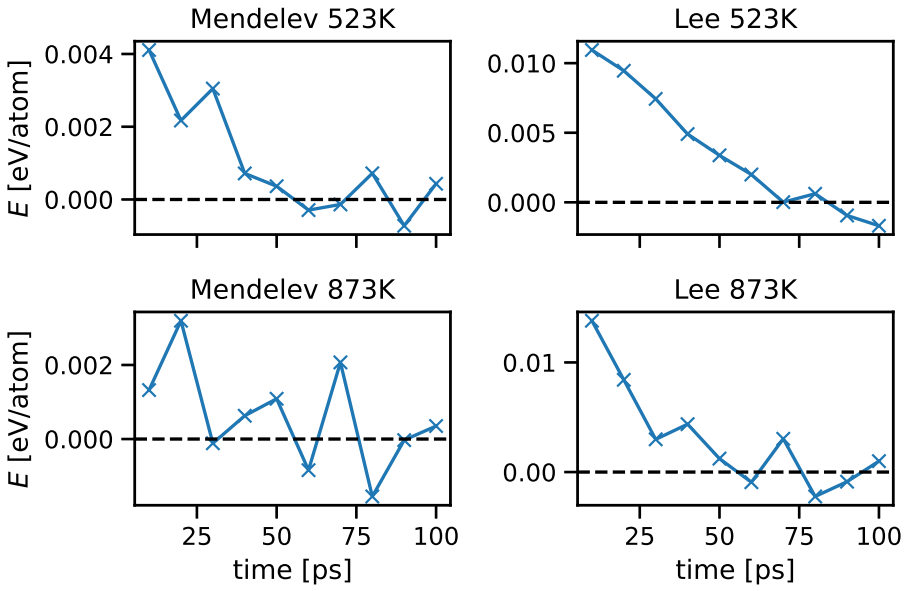

Figure 4: Potential energy convergence as a function of time (and thus MC swaps) for Mendelev [8] and Lee [10] potentials at high and lower temperture. Dashed line shows the average energy for the last five frames.

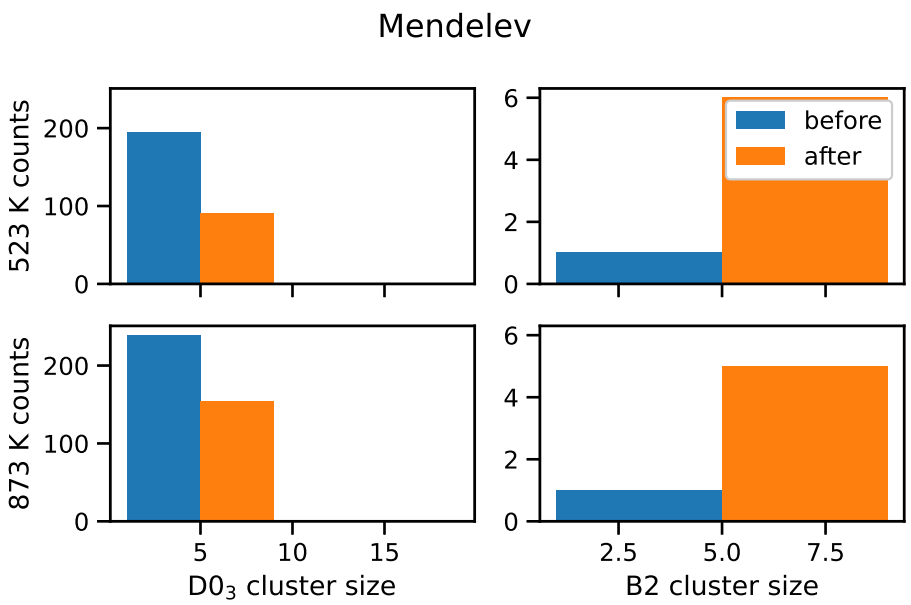

Figure 5: Cluster counts (ignoring single atom "clusters") for the Mendelev potential before (blue) and after (orange) MCMD equilibration from a random mixture, shown for $D0_3$ and B2 reference phases at two different temperatures.

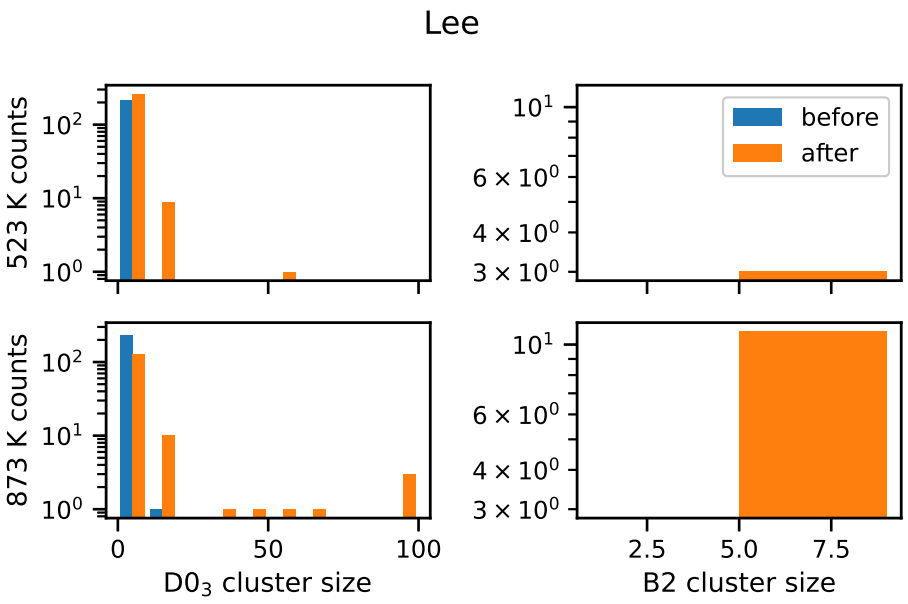

Figure 6: Cluster counts (ignoring single atom "clusters") for the Lee potential before (blue) and after (orange) MCMD equilibration from a random mixture, shown for $D0_3$ and B2 reference phases at two different temperatures. Binning is truncated at 100, so larger clusters are all lumped into the final bin shown.

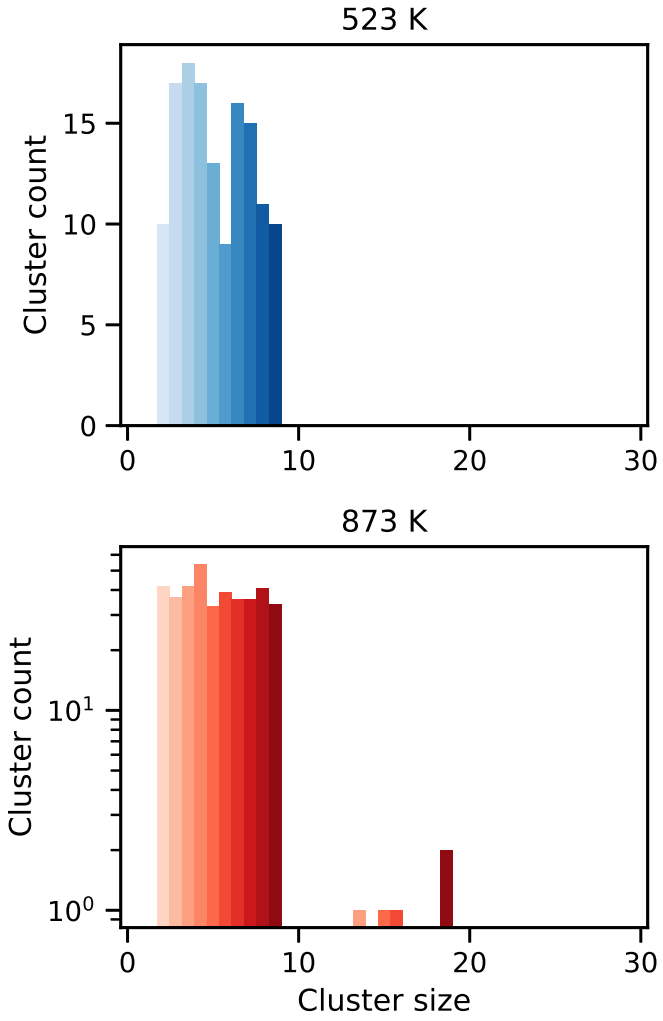

Figure 7: Identified $D0_3$ clusters evolving with the Lee potential from an initial state of full BCC-$D0_3$ phase separation. Results for (a) 523 K and (b) 873 K show evolution through time with darker bars being later in the simulation.

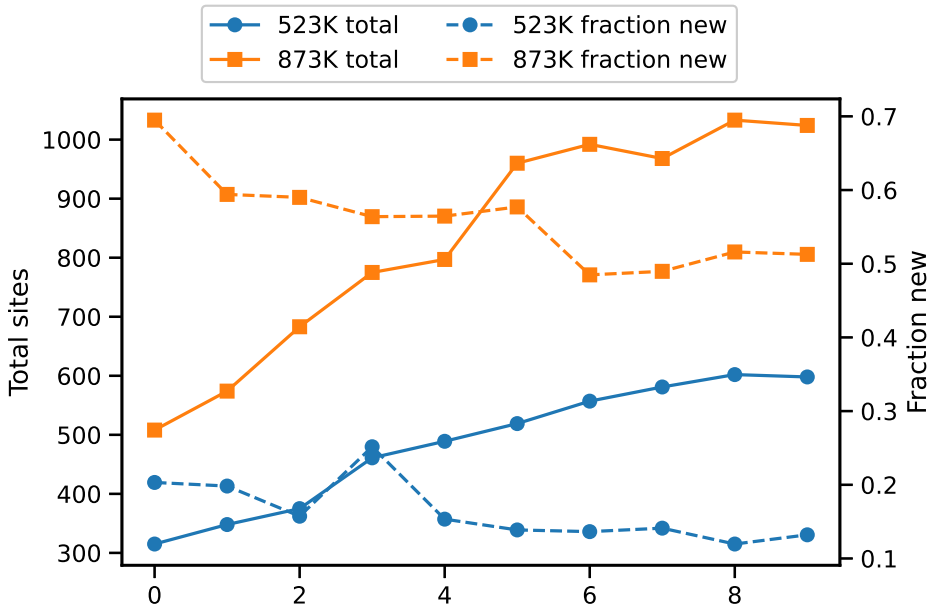

Figure 8: Total number of $D0_3$ sites identified at each frame (solid) (i.e. 10 ps MD time and 100 iterations of performing MC trials on 10% of the system) and the fraction of sites which were *not* in clusters in the last frame (dashed). Results shown for 523 K (blue circles) and 873 K (orange squares).

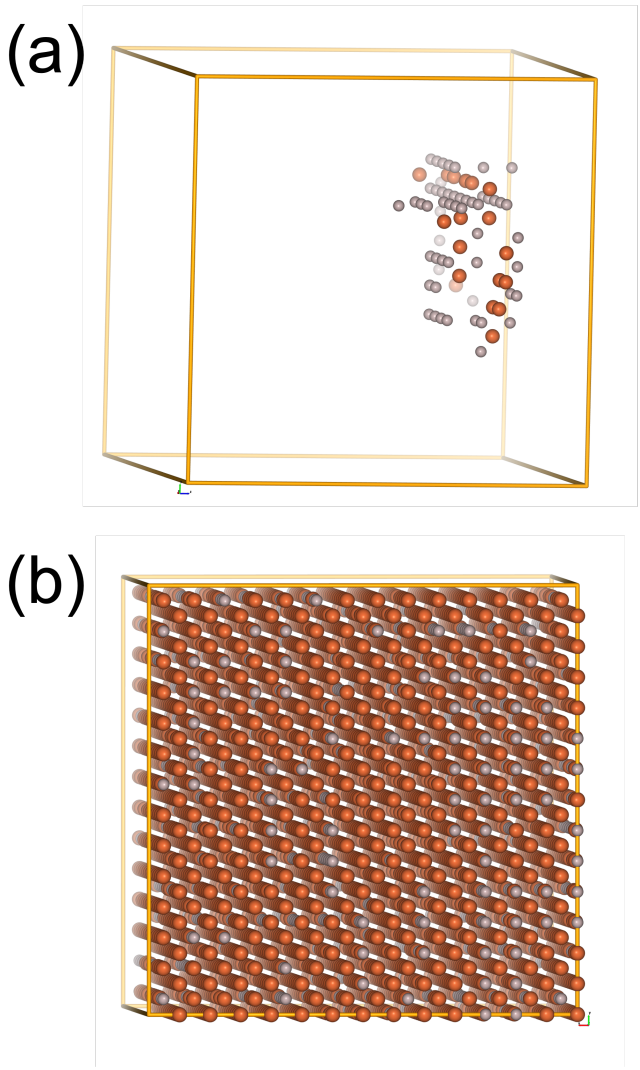

Figure 9: (a) one of the larger B2 clusters constructed with a more relaxed clustering condition of 11 NN and (b) the complete structure from the end of the MCMD equilibration with the Mendelev potential at 523 K.